Analysis of Efficiency and Axial Compensation in Continuous-Contact Helical Gear Pumps through Multiphysics Modeling and Experimental Validation

Parth Tawarawala[1,*], Harsh Kulkarni[1], Dinghao Pan[1], Andrea Vacca[1]

[1]*Maha Fluid Power Research Center, School of Mechanical Engineering, Purdue University, Lafayette, IN, USA*
E-mail: ptawaraw@purdue.edu
** Corresponding Author*

Abstract.

This work presents a multi-physics, strongly coupled numerical model for the study of continuous-contact helical gear pumps (CCHGP), specifically focusing on the numerical analysis of their axial compensation and the prediction of volumetric and hydromechanical efficiencies. The proposed work involves a multi-domain multi-physics modeling approach that combines lumped-parameter modeling of the fluid domain and body dynamics, with consideration of all degrees of freedom and range of motion of the floating bodies, and a CFD-based numerical model for the lubricating interfaces of the continuous-contact helical gear pump, built using an in-house C++-based framework, Multics. The paper shows that the model predicts the pump efficiency trends and outlet pressure ripple in good agreement with experimental measurements on a reference unit, while considerably improving upon state-of-the-art models, and reports a breakdown of the major loss sources in the pump. The paper also demonstrates model capabilities in predicting gear micro-motions and dynamics. The complete model can be used to perform predictive numerical simulations of existing designs or to optimize them to improve performance.

Keywords. Continuous-contact Helical Gear Pump; Multiphysics modeling; Axial Compensation dynamics; Efficiency prediction; Experimental Validation

1. INTRODUCTION

The Continuous-Contact Helical Gear Pump (CCHGP), shown in Figure 1.1, is a positive-displacement machine that has gained interest in the fluid power community for its low-noise operation, first introduced and studied in [1][2][3]. As noted in [4], specific geometric configurations of CCHGPs achieve a theoretical flow ripple of zero, thereby significantly reducing noise during operation. As hydraulic machines are being developed for new applications, such as electrification, pump noise must be addressed. This is particularly true for the External Gear Pump (EGP). CCHGPs share structural similarities with EGPs while addressing one of their biggest disadvantages; thus, they must be studied in detail for applications in hydraulic actuation and fluid transport.

The CCHGP, like the EGP, consists of a drive and driven gear, journal bearings to compensate for radial loading on gears, and lateral pressure plates for axial sealing and compensation. The transverse gear profile is a special compound profile called the continuum profile. However, there are critical differences as well. During meshing, the tips and roots of continuum gears seal completely, creating a pressure-differential sealing surface in the axial direction, a feature absent in EGPs. The helical gear design introduces unbalanced axial loads and tilting moments that affect axial gap heights and bushing dynamics. Furthermore, CCHGP units often utilize pressurized pistons to compensate for the gears' axial imbalances. These pistons introduce leakage paths from the high-pressure port to the low-pressure drain, altering bearing dynamics and increasing volumetric losses. These complexities prevent the direct application of EGP design principles to CCHGPs, and dedicated tools are required to support the CCHGP's research and development.

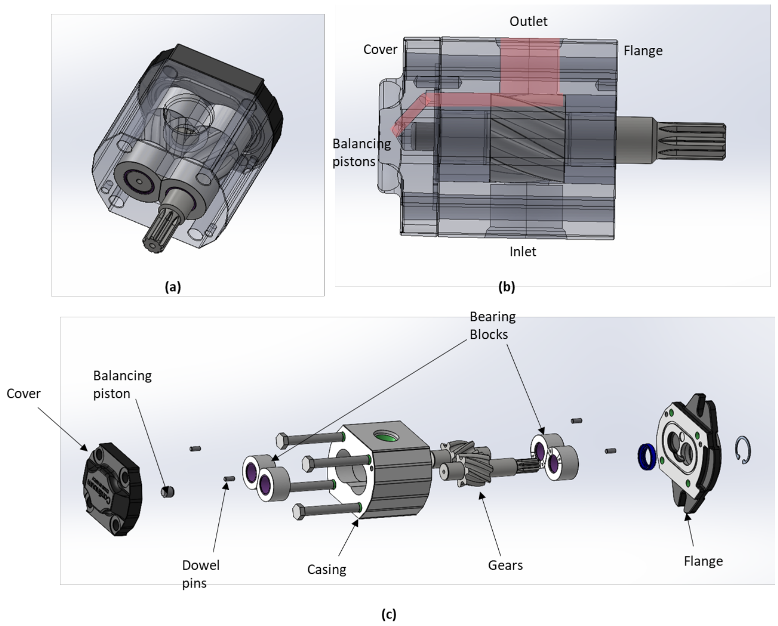

Figure 1.1. Reference CCHGP. (a) 3D CAD of the pump; (b) axial compensating system of the pump; (c) exploded view of the components.

Previous analytical models have correlated gear profiles with performance parameters such as compactness and flow ripple [5][6], but they fail to predict losses due to leakage, compressibility, and cavitation. Lumped Parameter Models [4] can capture the physics of these fluids while enabling very fast evaluation times. However, these models struggle to accurately capture the compensation mechanisms and lubricating interfaces. Similarly, 3D CFD [7] methods often simplify body dynamics and lubrication interfaces, limiting their utility for predicting failures of compensation mechanisms and associated losses.

State-of-the-art numerical multi-physics models, such as the Multics suite developed by the authors' lab [8], address these limitations by coupling compressibility, leakage, cavitation, body dynamics, contact, and thermal effects. While the Multics-HYGEsim model for EGPs [9][10] is a strong candidate for direct application here, the CCHGP's unique gear morphology and complex axial compensation require a dedicated multi-physics model development and investigation. Furthermore, the loss distribution in CCHGPs is expected to differ from that of EGPs and is thus described in a dedicated section in this paper.

Earlier studies [4][11] established an understanding of CCHGP operation but neglected the dynamics of the axial gear and bushing body, as well as piston-interface leakage. The model in [12] calculates static axial forces but neglects the dynamic motion and behavior of the compensation system and the lateral interface. The axial compensation system controls lateral gap heights, which directly affect volumetric and torque losses; thus, accurately modeling its dynamic behavior is essential. This paper addresses these gaps by incorporating axial compensation dynamics, meshing friction, and piston leakage into a strongly coupled multi-physics model. This detailed simulation also enables precise analysis of the breakdown and distribution of energy loss, which is validated against experimental results in this paper. Such insights enable direct comparison with EGP loss mechanisms [10]. This model enables hydraulic machine experts who might retrofit EGP housings with continuum gearsets to optimize tolerances and fluid-dynamic features for CCHGPs.

The primary novel contributions of this paper are: (i) The implementation of a strongly coupled multi-physics model for a CCHGP; (ii) Detailed modeling of axial compensation dynamics, film contact and friction losses, meshing friction forces, and axial piston leakage, with results compared against state-of-the-art methods; and (iii) Experimental validation of the model's efficiency and ripple predictions. The remainder of this paper describes the reference CCHGP geometry (Section 2), details the multi-physics model (Section 3), presents results and validation (Section 4), and concludes with key findings.

2. CCHGP Geometry Description

The reference CCHGP (Figure 1.1) consists of the following components:

1. **Drive gear:** Connected via spline to the prime mover.
2. **Driven (slave) gear:** In mesh with the drive gear.
3. **Top bushing:** Located on the gear spline side.
4. **Bottom bushing:** Located opposite the spline side.
5. **Axial piston:** Situated within the casing bottom cover for axial compensation.

The CCHGP employs a compound circular arc-involute 'continuum' profile. Unlike standard truncated involute profiles used in EGPs, this geometry ensures a continuous transition of the contact point throughout the meshing cycle, eliminating sudden transitions as new tooth pairs engage [1]. The conjugate root and tip geometry provide almost complete sealing in both tangential and axial directions, reducing the displacement chamber dead volume to near zero. Because this transverse profile yields a low contact ratio (CR), a helix angle is used to achieve a total CR greater than 1; this helix also allows a smooth transition between low and high pressures. Furthermore, the helix causes the root-tip sealing surface to move axially during rotation, creating a secondary compression mechanism. These features yield a theoretical kinematic ripple of zero [4]. However, factors such as axial micromotions, leakage, and compressibility result in a small but non-zero real-world ripple.

Similar to a standard involute EGP's construction, floating bushings are present on either side of the gearset to maintain axial sealing. Each bushing is hydrostatically balanced by a pressurized chamber on its outer axial face, which counters the fluid pressure from the gear side. Because the gear-side forces fluctuate while the balancing force remains static, the bushings' position and orientation vary continuously. Due to the helix angle, the top and bottom bushings experience asymmetric loading, which must be accounted for in the pump's design and modeling. Additionally, each bushing houses two journal bearings, one for each gear that supports the radial loads acting on the gears and shafts. The materials and surface roughness of these components are generally the same as those used for a standard EGP. The reference unit has split bushings in which the two halves of the bushing compensate each gear independently. Some CCHGP designs instead use a single bushing for the same.

To compensate for the axial load imbalance on the gears caused by helical asymmetry, the reference unit uses axially oriented pistons in the casing bottom cover. The far end of these pistons is pressurized by HP port fluid (see Figure 1.1(b)). These pistons push the axial face of the gear shaft. This compensating force is static, whereas the gears' axial loading is dynamic due to gear motion and film forces. Multiple design variations exist for this axial compensation of gears, using 2 pistons (one for each gear) or 1 (for the drive gear), with some designs even substituting pressurized fluid for pistons to compensate the gears directly. The reference unit consists of one piston pushing on the drive gear. The piston floats freely with clearance, and thus there is leakage from the piston's far-side chamber towards the bushing, into the journal bearings, and eventually into the drain. In this case, the slave gear is axially compensated by the gear-meshing force, which varies over time. This complex axial motion requires detailed modeling of the axial forces on the gears. While the current model analysis is presented for a single-piston design, its versatility allows the study of these different compensation mechanisms with minor adjustments.

3. MULTI-PHYSICS CCHGP MODEL

The CCHGP Multics model is a C++-based, multi-domain, multi-physics model comprising fluid, lubrication, and solid domains. These domains have individual solvers that communicate with each other at each solver step. The three domain solvers solve their respective physics and also exchange information with one another, as described in Figure 3.1. The novelty of this paper lies not in introducing individual solvers, but in demonstrating how they can be integrated to model the performance aspects of a CCHGP. For further details on individual model solvers and their strong coupling, readers are encouraged to refer to [8]. In Figure 3.1, the model physics in black were presented in earlier publications [11], while the features marked in red are the novel contributions of this paper. The solver implementations specific to CCHGP are described briefly in this section.

3.1. Fluid domain modeling

The fluid domain is modeled using a lumped-parameter approach that forms a hydraulic circuit of chambers and flow connections, consisting of 3 component types [4].

Chambers: These are lumped volumes of fluid with uniform state and physical properties. Their governing equation is the isothermal pressure build-up equation (equation (3.1)).

$$\frac{dp_{CV}}{dt} = \frac{K_{CV}}{V_{CV}}\left(\frac{\sum m_i}{\rho_{CV}} - \frac{dV_{CV}}{dt}\right) \tag{3.1}$$

This equation is isothermal. It can account for cavitation and aeration, but it is static, with no time delays or hysteresis effects due to bubble formation/collapse. The model can account for pressure-dependent variations in fluid properties by importing tabulated values, which are interpolated at each solution step. In the CCHGP, the chamber of interest is the Tooth Space Volume (TSV), which is the space between a tooth pair, the outer casing, and the axial sealing surface. The fluid inside the TSV compresses to high pressure to achieve positive displacement. The formulation of TSVs is described in detail in [4].

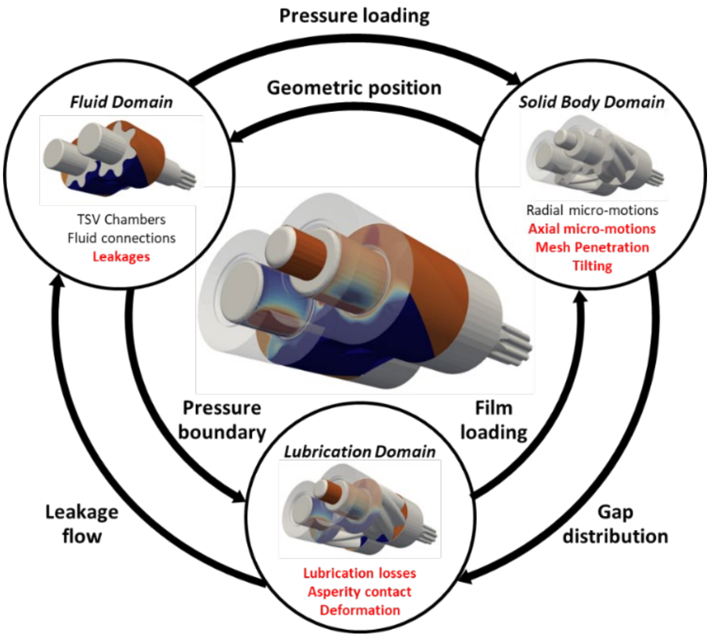

Figure 3.1. Multi-Physics model overview for CCHGP

Orifice connections: The TSVs are connected to each other and to the outlet/inlet ports through fluid connections modeled as orifices, with physics governed by the modified turbulent orifice equation (equation (3.2)).

$$Q_{i,j} = C_q \Omega \sqrt{\frac{2(p_i - p_j)}{\rho}} \operatorname{sign}(p_i - p_j) \tag{3.2}$$

Piston leakage: The piston interface introduces an additional leakage, modeled as a hydraulic circuit. Figure 3.2 shows the leakage path and circuit for a single-piston pump. The flow connections here are modeled as lubrication films as described in Section 3.2.

Tip leakages: The leakage due to radial clearance between gear tooth tip and casing is important because: (a) it leads to volumetric losses in the pump; (b) it controls the pressurization timing of TSVs. For standard involute EGMs, this flow is modeled as a parallel-plate flow [10]. However, since the tip leakage path of the CCHGP is a curved constriction, it is modeled using the approach presented in [13]. The instantaneous local tip gap is calculated from the gears' radial motion and tilting, as explained in Section 3.3.

Geometric preprocessing: The geometric properties used here: chamber volume (V_{cv}) and orifice flow area (Ω) vary with time, but depend only on pump construction, not operating conditions. A geometric preprocessor calculates and stores this information for interpolation during the simulation, to save time. This geometric preprocessing for CCHGPs is described extensively in [4].

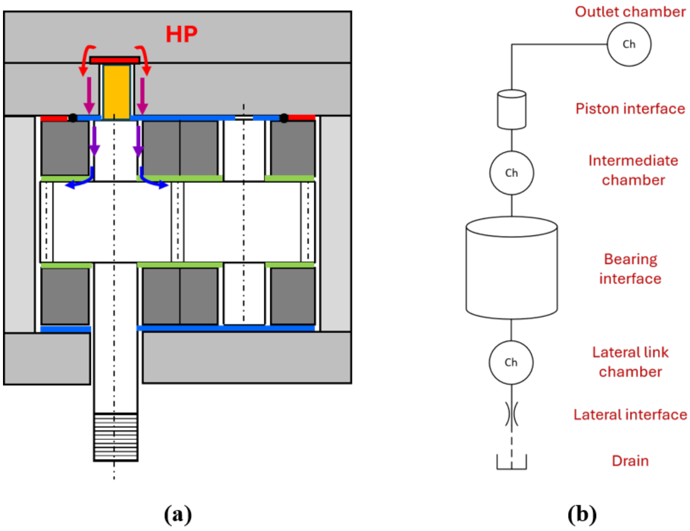

Figure 3.2. (a) Piston leakage path inside the pump, (b) Model hydraulic circuit

3.2. Lubrication interface modeling

Lubricating interfaces are responsible for load bearing and hydrodynamic support. Two consequences of these interfaces, due to their often-small gaps, are volumetric losses from flow leakage and torque losses from shear and contact. These effects were simplified in previous CCHGP models but are modeled here using a numerical 2D CFD approach. The governing equation for fluid-structure interaction effects in lubricating interfaces is the Universal Mixed Reynolds Equation [8] (Equation (3.3)).

$$\nabla \cdot \left(\phi_p \left(\frac{K_T h^3}{12\mu} \nabla \rho\right)\right) = \nabla \cdot \left(\rho \overrightarrow{v_m} \left(\phi_R R_q + \phi_c h\right)\right) + \nabla \cdot \left(\rho \phi_s R_q \left(\frac{\overrightarrow{v_t} - \overrightarrow{v_b}}{2}\right)\right) + \frac{\partial \rho \left(\phi_R R_q + \phi_c h\right)}{\partial t} \quad (3.3)$$

This equation is isothermal. It can account for both static cavitation and variations in fluid properties with pressure. This model also accounts for the effects of mixed lubrication and surface asperities on pressure build-up and effective gap height.

The source term in this equation is the instantaneous, local gap height at the interface. $\left(\bar{h}(x, y, t)\right)$. This gap height is influenced by 3 factors:

Rigid body linear and angular motion of the bodies: The motion of the bodies is integrated and solved at each time step and is described in detail in Section 3.3.

Deformation of the solid body surface: This uses an analytical approximation in which the solid bodies are modeled as infinite half-planes [8]. More sophisticated numerical techniques exist [8] that drastically increase computation time. Therefore, to study performance trends of the axial compensation, an analytical approximation of deformation is used.

Surface roughness and asperities: Mixed-lubrication effects are considered using the method proposed by Patir and Cheng [14]. This method defines flow factors based on statistical characteristics of surface roughness to quantify their effect on flow rate. In the case of surface asperity contact, local contact pressure and solid asperity friction are also calculated from the local gap height using the formulation proposed by [15]. This component is critical for modeling contact in conditions such as over-compensated bushings.

The details of the exact calculations can be found in previous publications by the authors' lab [8] and are therefore not repeated here. Similar to EGPs, there are two specific geometries of lubricating films: (a) polar films for the lateral interface between gear and bushing axial surfaces and (b) cylindrical films for the journal bearings. Additionally, the piston and casing form a cylindrical film with its own dynamics and leakage, which are modeled as an independent Reynolds film with chamber boundary conditions from the piston leakage circuit introduced in Section 3.1.

3.3. Solid domain modeling

The solid bodies float freely in the pump, exhibiting micro-motions. These micro-motions control the instantaneous local gap heights at the lubricating interfaces, thereby directly affecting load-bearing capacity, leakage, and torque losses.

The dynamics of each floating body are governed by Newton's 2nd law of motion for translation and rotation. The equations are solved by adding them to the global system of ODEs and then integrating the resulting system. However, it is important first to understand and calculate the net forces ($\sum F_i$) and moments ($\sum M_i$) acting on each specific component.

Drive and slave gears: The gears are capable of 4 types of movement, corresponding to their 6 degrees of freedom.

(i) Radial/transverse micro-motions of the gears inside the bearing (x, y).
(ii) Tilting of the gears with respect to the nominal bearing orientation (θ_x, θ_y).
(iii) Axial micro-motion of the gears (z).
(iv) Relative rotation/penetration of the gears (θ_z).

The previous CCHGP model [11] neglects motions (iii) and (iv), while simplifying (ii) due to the absence of coupling between body dynamics and lubricating interfaces. This paper relaxes these assumptions by modeling all of the gears' DOFs and quantifying their effects. This is crucial to accurate performance estimation of the axial compensation.

The forces acting on the gears in radial and axial directions are shown in Figure 3.3. These can be classified into 4 sources: (a) TSV pressure forces; (b) Lubricating gap pressure and shear forces; (c) Piston axial compensation forces; (d) Meshing contact and friction forces.

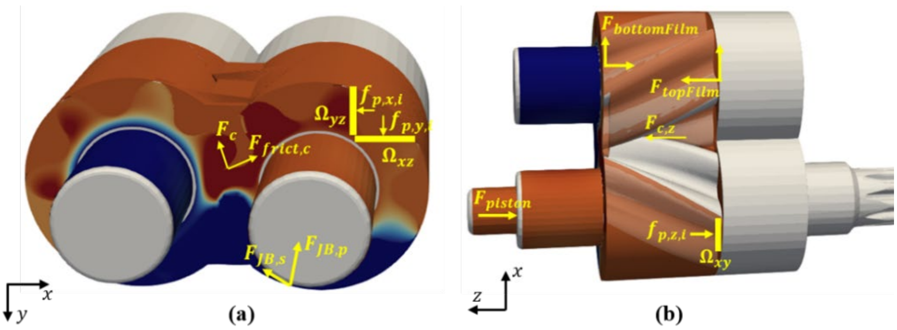

Figure 3.3. Forces acting on gears (a) radially, and (b) axially

TSV pressure loading depends on the TSV projection areas on the gears and their moment arms in the (x, y, z) directions. These quantities are calculated and stored by the geometric preprocessor [4].

The lubricating interfaces (journal bearing and lateral gap) exert both normal and tangential forces relative to the solid body surface. Normal forces arise from fluid-film pressure or contact, and tangential forces comprise film shear and asperity friction. Interface pressure calculations are handled by the lubrication interface solver (Equation 3.3). The film friction loss calculations are described in Equation 3.4.

$$\vec{F}_{fric} = \int \vec{\tau} \cdot d\vec{A} + \int P_c \left(-\frac{\vec{v}_t - \vec{v}_b}{|\vec{v}_t - \vec{v}_b|} \right) \cdot d\vec{A} \tag{3.4}$$

The first term represents viscous shear, while the second represents asperity contact friction.

The pistons apply an axial compensating force to the gear, modeled as a simple static force acting independently on each gear.

The gear meshing contact force is modeled as a spring-damper system based on the relative penetration between the gears. It is assumed that contact occurs only in the involute section of the drive flanks. The equation of force is given by Equation 3.5.

$$F_{contact} = k\delta + c\dot{\delta} \tag{3.5}$$

The teeth meshing penetration (δ) is the superposition of 2 effects: relative angular rotation of the gears about the z-axis and axial micro-motions of the gears. The penetration velocity $(\dot{\delta})$ is obtained by taking the time derivative of the instantaneous penetration (Equation 3.6).

$$\delta = r_{base} \Delta\theta_z \cos(\beta) + \Delta z \sin(\beta) \left(-\mathrm{sign}\left(\Phi_{\mathrm{helix}}^{\mathrm{drive}} \right) \right) \tag{3.6}$$

The stiffness and critical damping ratio of the contact are calculated using Hertzian theory.

Once the force is calculated, the moment on the gears due to contact forces can be determined from the 3D geometric location of the contact point.

Lastly, the friction forces (Equation (3.7)) and, subsequently, the moments are calculated using a coefficient of friction, with the correlation for EHL line contact based on [16].

$$F_{friction} = \mu_{EHL} F_{mesh} \tag{3.7}$$

The friction coefficient depends on fluid viscosity, which can change by orders of magnitude due to density changes in the contact region [16]. The model can input tabulated variations in fluid properties and therefore accurately model this behavior during meshing.

The drive gear is assumed to be rotating with a constant z-axis rotation velocity, and any torque imbalance is overcome by the prime mover. The slave gear is free to spin around its z-axis, with its angular position affecting the penetration. All other degrees of freedom for both gears are allowed, and their linear and angular positions are independently determined by integrating and solving the body-dynamics ODEs.

An important distinction between EGPs and CCHGPs is the tooth tip torque loss. As demonstrated in [10], tooth-tip losses contribute significantly to the overall loss of EGPs. In the case of the CCHGP, the hydrodynamic shear stress from tip-leakage flow acts on a very small area, contributing very little to the overall torque loss. Although this torque loss is modeled, it is not reported because its effect is negligible.

Top and bottom bushings: The lateral bushings control clearances with the gears' lateral surfaces by pressurizing the balancing chambers from behind, mimicking the pressure distributions of the gear TSVs and the lateral lubricating film. However, the compensation force is static, whereas the gear-side force varies over time. This leads to dynamic periodic motion in the bushing. The bushing is expected to be in contact with the casing in the LP region, resulting in a frictional force during its motion, which is applied as an external force on the bushing. To simplify the body dynamics, the current model assumes the split bushing halves move together without relative separation or tilt. Modeling the independent half bushings is out of scope for this paper.

4. RESULTS AND DISCUSSION

This section will describe the simulations conducted on a reference CCHGP unit. This is a 20 cm^3/rev 7-tooth pump with one-piston compensation. For confidentiality reasons, the design dimensions of the tested pump have not been disclosed. However, the tested pump was opened, and precision metrological measurements were taken to recreate the pump for simulations.

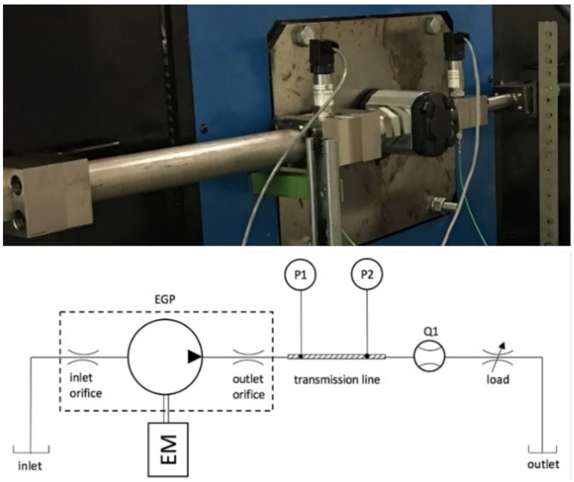

(a)

(b)

Figure 4.1. (a) Maha Multi-Purpose Test Rig with CCHGP, (b) Test circuit.

Sensor	Model
Outlet Pressure	Wika S-10
Inlet Pressure	Wika A-10
Pressure Ripple	PCB Piezotronics 108A02
Flow rate	VSE VS 4 Gear flowmeter
Shaft torque	HBM T10FS Torquemeter

Table 4.1. Sensors used for experimental measurements

To validate the model experimentally, tests were conducted using a steady-state test setup at the authors' lab, as shown in Figure 4.1. The focus of these experiments is to demonstrate how the model captures macroscopic trends in efficiency under certain reference operating conditions as supported by experimental validation. In the future, the authors aim to incorporate additional results for a larger range of operating conditions. The simulations and experiments were conducted at a fixed temperature of 50 °C, with ISO VG 46 hydraulic oil as the fluid. The sensors used in the experiments are listed in Table 4.1.

4.1. Efficiency results

The steady-state efficiency trends of the pump were compared across experiments, the current simulation model, and the baseline simulation model proposed in [11] at different pressures and a fixed speed of 2000 RPM. The differences in the model assumptions are summarized in Table 4.2. The results are plotted and compared in Figure 4.2.

Parameters/Assumptions	Baseline	Proposed
Gear axial (Z) motion & compensation	Fixed	Solved dynamically
Bushing axial (Z) motion	Fixed	Solved dynamically
Lateral film gap heights	Assumed symmetric	Solved independently
Film contact & mixed lubrication	Ignored	Solved
Deformation	Ignored	Solved
Gear meshing penetration & friction	Ignored	Solved
Piston interface leakage	Ignored	Solved

Table 4.2. Model assumption comparison between the baseline and the proposed.

The volumetric efficiency prediction has improved for some operating conditions while preserving trends; however, some discrepancies remain. The current model assumes a single-bushing design with simplified DOFs and deformation. Furthermore, the meshing flow connections are modeled as simple orifices, and the effects of gear tilting and manufacturing tolerances are ignored, all of which may affect the predicted volumetric efficiency. Future versions of the model can aim to address these assumptions.

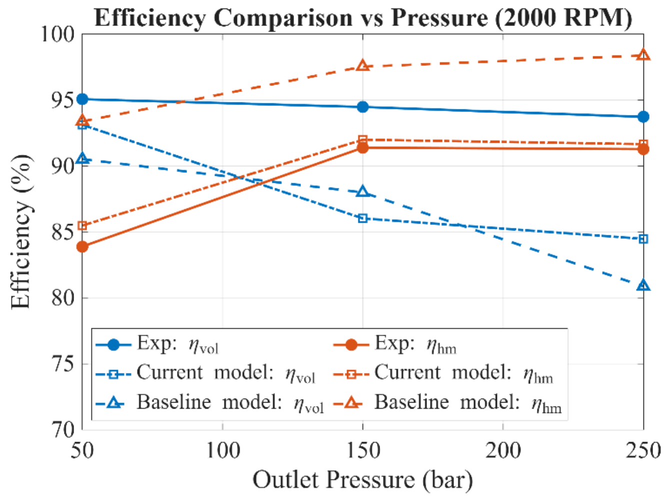

Figure 4.2. Comparison of hydromechanical (in red) and volumetric (in blue) efficiencies for the CCHGP between experiments and simulation models.

The hydromechanical efficiency prediction has improved significantly compared to the baseline model. To investigate this further, the mechanisms of torque loss are analyzed. There are 3 major torque-loss sources in the CCHGP: lateral lubrication, meshing, and journal bearing losses. The currently proposed model in this paper can model these losses, and their breakdown is presented here. The torque loss at the pump shaft seal is ignored in this model. The torque loss breakdown is presented in Figure 4.3. From the figure, it is clear that while the gear meshing and JB film loss predictions are largely consistent across models, the lateral film torque loss differs significantly. The baseline model severely underpredicts the lateral film losses compared to the current model.

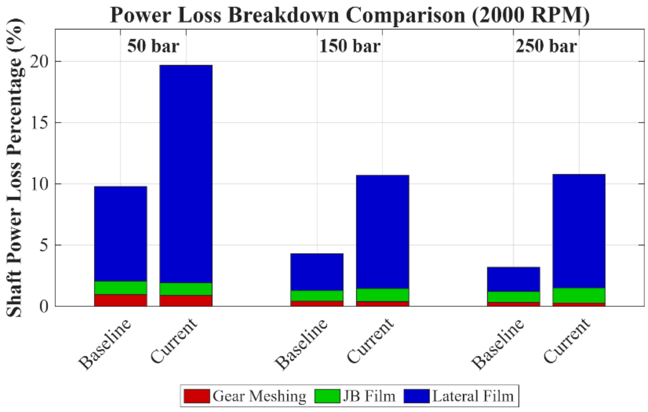

Figure 4.3. Distribution of torque losses as predicted by each model.

From Table 4.2 it can be seen how these model assumption relaxations contribute to better model predictions. Solving gear and bushing motion dynamics allows accurate estimation of the lateral gap height distribution, and a mixed-lubrication model in the films enables more accurate estimation of asperity friction losses. To demonstrate this, a more detailed breakdown of gap height distribution is needed.

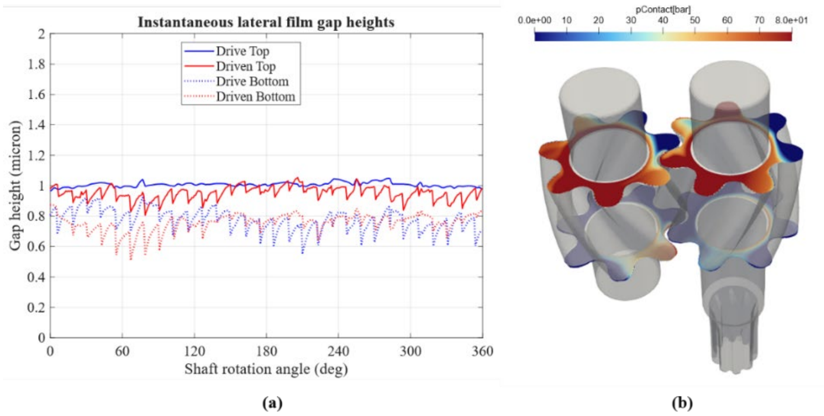

Figure 4.4. (a) Instantaneous minimum lateral gap heights predicted by the model ($\boldsymbol{\Delta P} = \mathbf{250}\ \boldsymbol{bar}, \boldsymbol{N} = \mathbf{2000}\ \boldsymbol{RPM}$), (b) Contact pressure in lateral films

The baseline model assumes a fixed, uniform rigid gap height at the lateral interface. For this simulation, the gap height is set to 1.5 microns to model full hydrodynamic lubrication, as assumed in [11]. However, in the proposed model, all 4 bodies (2 gears and 2 bushings) are allowed to move axially and deform. The resulting gap heights thus fall within the mixed-lubrication regime (see Figure 4.4(a)), leading to a buildup of contact pressure at the lateral interface (see Figure 4.4(b)). Surface asperity contact and friction increase the opposing torque exerted by the lateral interface, thereby increasing hydromechanical losses. The contribution from surface asperity friction can be calculated as the difference between the lateral film losses of the Proposed model with contact and those of the Baseline model without contact. It can be seen here that under all 3 operating conditions, the asperity friction loss dominates the lateral film loss.

The current model can not only model this interaction to more accurately capture losses in the CCHGP but also predict the effectiveness of a compensation mechanism arising from body dynamics. This can be useful for conducting a sensitivity study on the bushing balance areas while designing them for CCHGP.

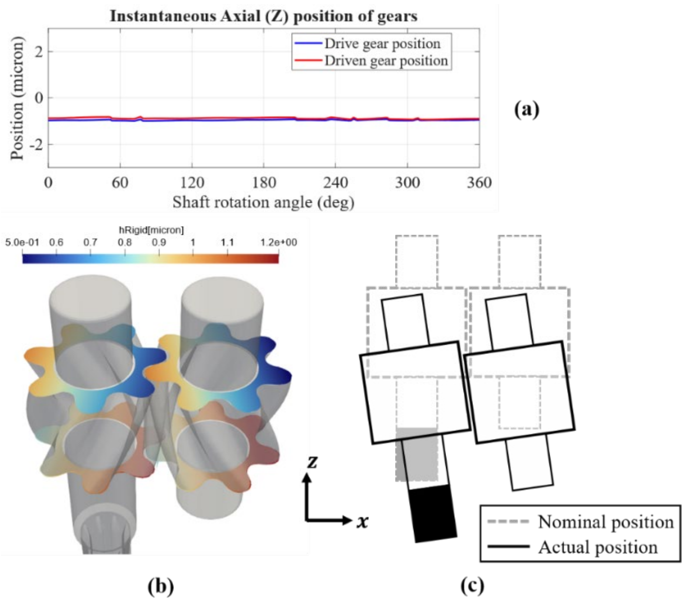

Figure 4.5. (a) Axial position of gears; (b) Lateral rigid gap heights showing tilting, (c) Comparison of the gears' nominal and actual positions (exaggerated)

4.2. Gear micro-motions

The model offers detailed insights into pump physics, some of which are presented here. Figure 4.5 shows the position of the gears as predicted by the model. It can be seen clearly that the gears tend to move axially towards $-z$ (towards the driveshaft) and away from the piston side, as expected from the orientation of the pressure force. Furthermore, the gap height distribution shows that both gears tilt in the same direction. Thus, the casing length must be designed to accommodate the gearset's range of motion, and any gear profile micro-corrections must also account for the magnitude of tilting.

4.3. Pressure ripple results

The model can also predict the pressure ripple, which can be compared to experimental results. For the experiments, a PCB Piezotronics Model 108A02 ICP Pressure Sensor was utilized to measure the outlet pressure ripple. The pressure ripple comparison between experiments and simulations for two operating conditions is shown in Figure 4.6. The results show good agreement between the simulated and experimental pressure ripples in amplitude and frequency. The difference can be attributed to the CCHGP's pressure ripple order-of-magnitude being much smaller than that of other pumps, making it more sensitive to factors such as external excitations, manufacturing defects, and sensor noise than most other measurements.

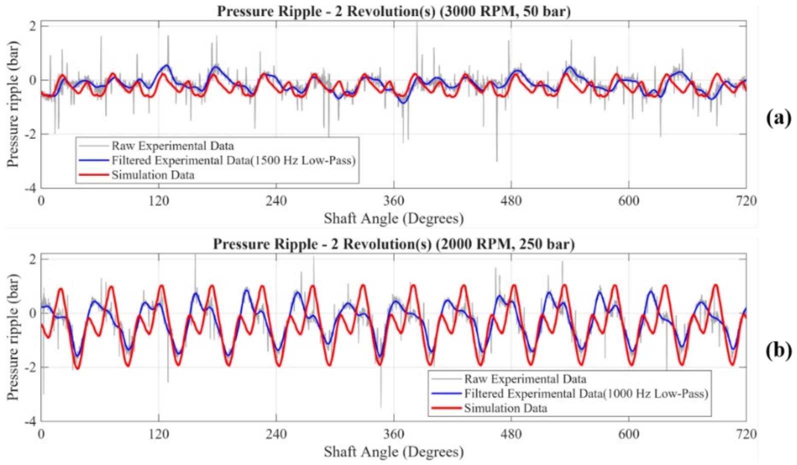

Figure 4.6. Comparison of pressure ripples from simulations and experiments for (a) $\boldsymbol{\Delta P = 50\ bar, N = 3000\ RPM}$, (b) $\boldsymbol{\Delta P = 250\ bar, N = 2000\ RPM}$

5. CONCLUSIONS

This paper presents a multi-domain, multiphysics numerical model for analyzing a Continuous Contact Helical Gear Pump. The novel additions to the model are presented, and the model was applied to a reference CCHGP unit as a case study, with experimental validation. The results show considerable improvement in predicting steady-state efficiency trends compared to state-of-the-art models. The hydromechanical efficiency trends now match experiments much more closely than state-of-the-art models. The volumetric efficiencies do not match as closely and will require a more in-depth investigation and modeling effort. A detailed breakdown of torque losses and their contribution to hydromechanical efficiency was also presented. Furthermore, the pressure ripple predicted by the model also shows good agreement with experiments. This model has applications in the design of axial compensation bushings and pistons for a CCHGP, as it can accurately predict losses at the lateral interface and the dynamics of the floating bodies. In the future, the authors intend to validate the model for more operating conditions. Furthermore, as with EGPs, the deformation of the bushing and casing can be captured more accurately using a numerical influence matrix approach. The authors also plan to conduct a detailed CFD analysis of leakage and flow in the meshing zone to understand volumetric losses better and improve the model's prediction of volumetric efficiency. The authors also plan to validate the simulation's prediction across multiple speeds in the future. The complete model is highly versatile and can provide users with detailed insight into pump operation to develop novel CCHGP designs.

6. REFERENCES

[1] K. Seki and K. Mitome, "A new continuous contact low-noise gear pump," *Journal of Mechanical Design*, vol. 105, no. 4, pp. 736–741, Dec. 1983, doi: 10.1115/1.3258544.

[2] M. A. Morselli, "Rotary positive-displacement pump with meshing gear wheels without encapsulation, and gear wheel for such a positive-displacement pump," US 6,769,891 B2, Aug. 03, 2004

[3] M. A. Morselli, "Mechanical and Hydraulic Noise of Gear Pumps: The Drastic Evolution Marked by 'Continuous Contact' Pumps."

[4] X. Zhao and A. Vacca, "Analysis of continuous-contact helical gear pumps through numerical modeling and experimental validation," *Mech. Syst. Signal Process.*, vol. 109, pp. 352–378, Sep. 2018, doi: 10.1016/j.ymssp.2018.02.043.

[5] H. Jang and S. Ji, "Numerical Study on the Instantaneous Theoretical Flow Rate of the Continuous Contact Gear Pump with a New Geometrical Approach," *J. Mar. Sci. Eng.*, vol. 12, no. 12, Dec. 2024, doi: 10.3390/jmse12122332.

[6] C.-K. Chen and S.-C. Yang, "Geometric modelling for cylindrical and helical gear pumps with circular arc teeth," *Proc. Inst. Mech. Eng. C J. Mech. Eng. Sci.*, vol. 214, no. 4, pp. 599–607, 2000, doi: 10.1243/0954406001523939.

[7] X. Zhao, A. Vacca, and S. Dhar, "Numerical Modeling of a Helical External Gear Pump With Continuous-Contact Gear Profile: A Comparison Between a Lumped-Parameter and a 3D CFD Approach of Simulation," in *Proceedings of the BATH/ASME 2018 Symposium on Fluid Power and Motion Control.*, ASME, 2018.

[8] T. Ransegnola, "A Strongly Coupled Simulation Model Of Positive Displacement Machines For Design And Optimization," PhD Thesis, Purdue University, 2020.

[9] A. Pawar, A. Vacca, and M. Rigosi, "Comparative Analysis of External Gear Machine Performance Considering Deformation and Thermal Effects," *International Journal of Fluid Power*, vol. 25, no. 4, pp. 465–492, 2024, doi: 10.13052/ijfp1439-9776.2543.

[10] A. Pawar, V. Harish, B. Manne, A. Vacca, and M. Rigosi, "Analysis of Torque Efficiency of External Gear Machines Considering Gear Teeth Roughness," *Mech. Mach. Theory*, vol. 199, Sep. 2024, doi: 10.1016/j.mechmachtheory.2024.105675.

[11] X. Zhao and A. Vacca, "Multi-domain simulation and dynamic analysis of the 3D loading and micromotion of continuous-contact helical gear pumps," *Mech. Syst. Signal Process.*, vol. 163, Jan. 2022, doi: 10.1016/j.ymssp.2021.108116.

[12] Y. fei Wu, P. qi Ge, and W. bo Bi, “Analysis of axial force of double circular arc helical gear hydraulic pump and design of its balancing device,” *J. Cent. South Univ.*, vol. 28, no. 2, pp. 418–428, Feb. 2021, doi: 10.1007/s11771-021-4612-2.

[13] R. Rituraj and A. Vacca, “Investigation of flow through curved constrictions for leakage flow modelling in hydraulic gear pumps,” *Mech. Syst. Signal Process.*, vol. 153, May 2021, doi: 10.1016/j.ymssp.2020.107503.

[14] N. Patir and H. S. Cheng, “An Average Flow Model for Determining Effects of Three-Dimensional Roughness on Partial Hydrodynamic Lubrication,” *J. Tribol.*, pp. 12–17, 1978.

[15] S. C. Lee and N. Ren, “Behavior of elastic-plastic rough surface contacts as affected by surface topography, load, and material hardness,” *Tribology Transactions*, vol. 39, no. 1, pp. 67–74, Jan. 1996, doi: 10.1080/10402009608983503.

[16] B. J. Hamrock, S. R. Schmid, and B. O. Jacobson, *Fundamentals of Fluid Film Lubrication*. CRC Press, 2004. doi: 10.1201/9780203021187.